Supplementary Materials

Anion-participating solvation enables compositionally graded interphases for durable subzero lithium-ion batteries

Shouxun Peng[1], Qing Yin[1,*], Bin Zhang[1], Zeyu Zhao[1], Meiyu Shi[1], Xiwen Li[1], Zheng Li[1], Bin Xiao[1], Xiuquan Gu[1], Mingjia Zhi[2], Eugene Chubenko[3], Vitaly Bondarenko[3], Hanna Bandarenka[3], Yang Pan[4], Shan Hua[4], Yanwei Sui[1,*]

[1]School of Materials and Physics, China University of Mining and Technology, Xuzhou 221116, Jiangsu, China.
[2]School of Materials Science and Engineering, Zhejiang University, 866 Yuhangtang Road, Hangzhou 310058, Zhejiang, China.
[3]Belarusian State University of Informatics and Radioelectronics, P. Browka Str. 6, Minsk 220013, Belarus.
[4]Guoneng Nanjing Electric Power Testing and Research Co., Ltd., Nanjing 210046, Jiangsu, China.

Correspondence to: Prof. Qing Yin, Prof. Yanwei Sui, Jiangsu Province High-efficiency Energy Storage Technology and Equipment Engineering Laboratory, School of Materials Science and Physics, China University of Mining and Technology, Xuzhou 221116, Jiangsu, China. E-mail: qingyin0715@cumt.edu.cn; suiyanwei@cumt.edu.cn

Table S1 Detailed compositions of electrolyte formulations investigated in this work.

Electrolyte formulation	Salt composition	Solvent/Diluent composition	Volume ratio (v/v)	salt-to-DMS/FEC ratio
LiDFOB + DMS/HFE/FEC	1.5 M LiDFOB	DMS/HFE/FEC	5:4:1	1:4.85
$LiPF_6$ + EC/DMC	1.0 M $LiPF_6$	EC/DMC	3:7	N.A.
$LiBF_4$ + DMS/HFE/FEC	1.5 M $LiBF_4$	DMS/HFE/FEC	5:4:1	1:4.85
$LiPF_6$ + DMS/HFE/FEC	1.5 M $LiPF_6$	DMS/HFE/FEC	5:4:1	1:4.85
LiDFOB + DMS/HFE	1.5 M LiDFOB	DMS/HFE	5:4	1:4.35
LiDFOB + DMS/ FEC	1.5 M LiDFOB	DMS/ FEC	5:1	1:8.08
LiDFOB + HFE/FEC	1.5 M LiDFOB	HFE/FEC	4:1	1:1.87
LiDFOB + EC/DMC	1.5 M LiDFOB	EC/DMC	3:7	N.A.
$LiBF_4$ + PC/DME	1.0 M $LiBF_4$	PC/DME	1:1	N.A.

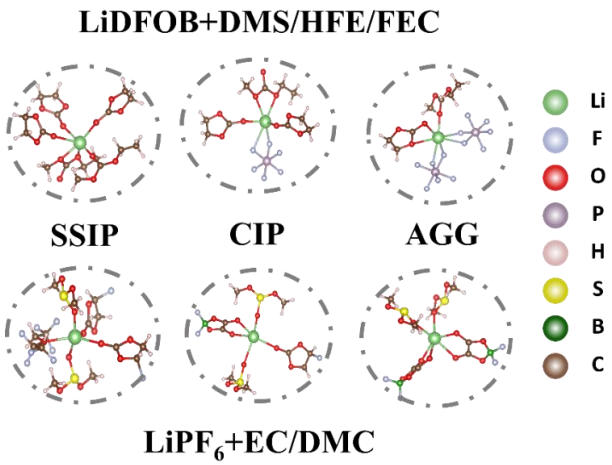

Figure S1. Solvation structure distributions of SSIPs, CIPs and AGGs.

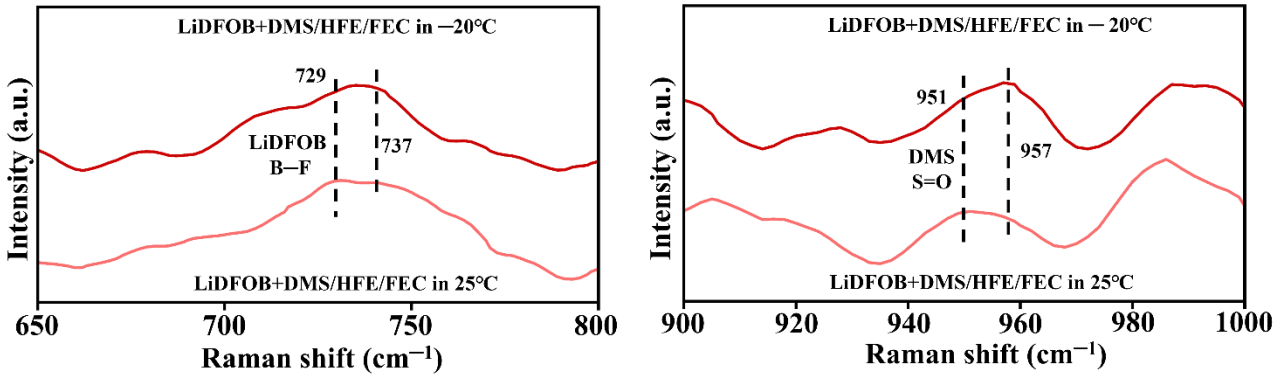

Figure S2. Local magnification of Raman spectra for LiDFOB+ DMS/HFE/FEC electrolyte.

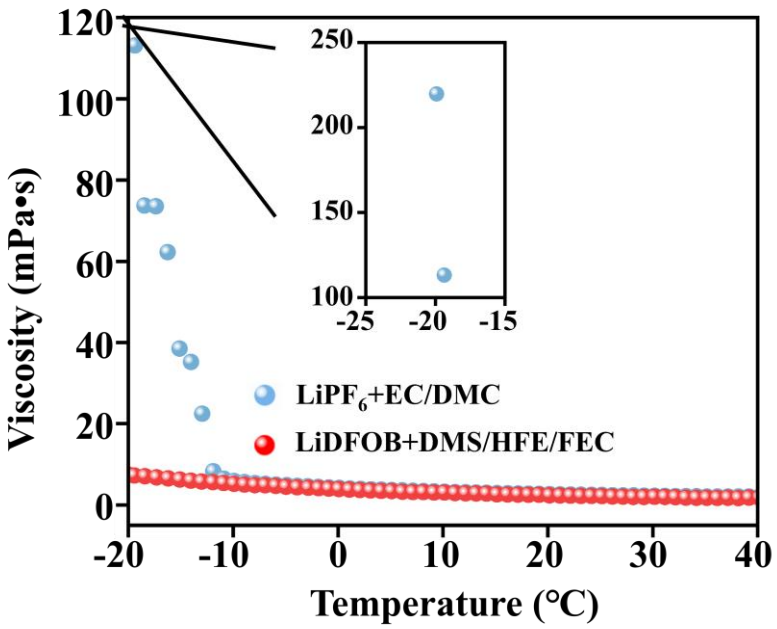

Figure S3. Viscosity of different electrolytes.

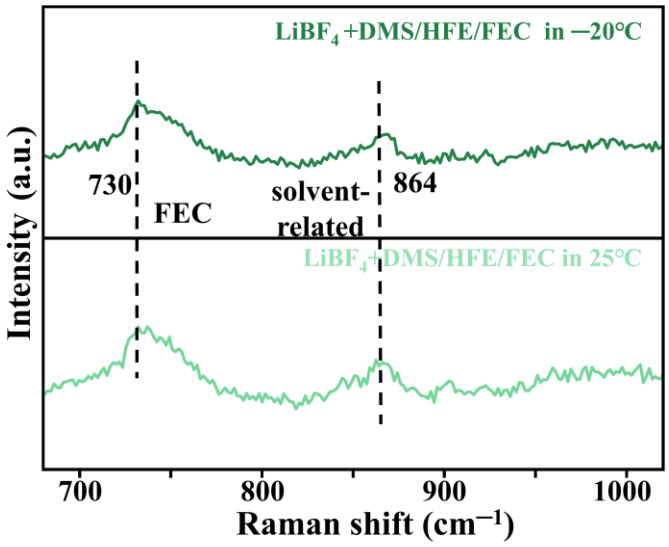

Figure S4. Local magnification of Raman spectra for $LiBF_4$ in DMS/HFE/FEC solvent environment at different temperatures.

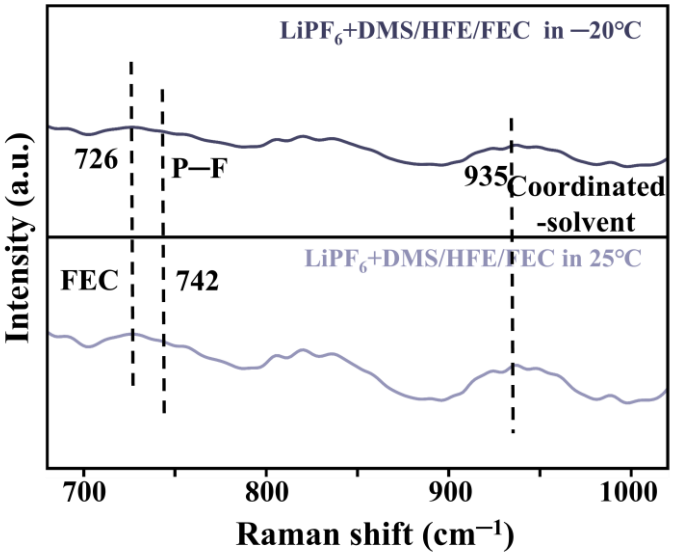

Figure S5. Local magnification of Raman spectra for $LiPF_6$ in DMS/HFE/FEC solvent environment at different temperatures.

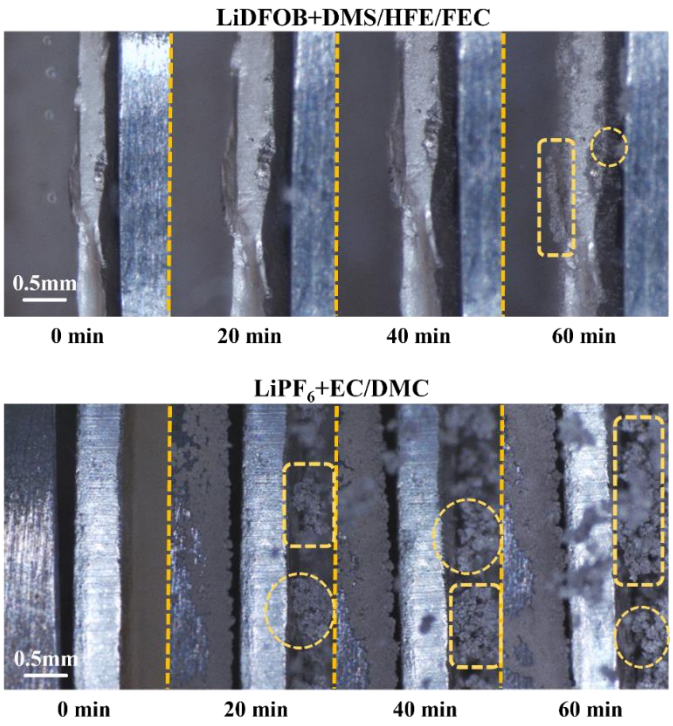

Figure S6. *In-situ* dendrite distribution on the surface of lithium anode at different cycling times.

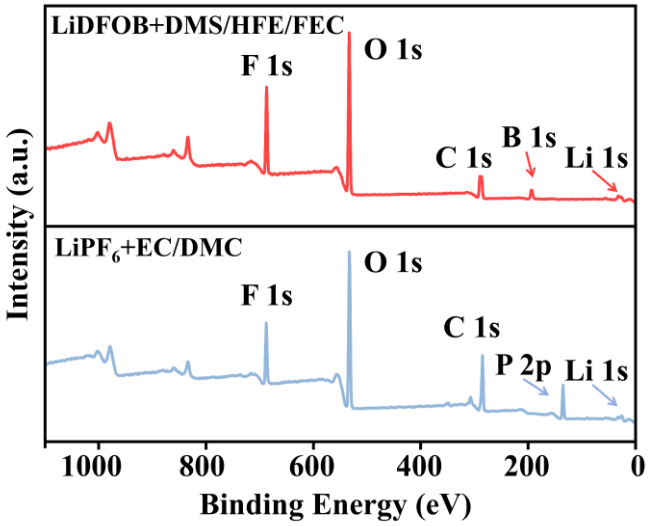

Figure S7. XPS survey spectra of electrolyte derived residue films obtained from LiDFOB+DMS/HFE/FEC and $LiPF_6$+EC/DMC after vacuum treatment.

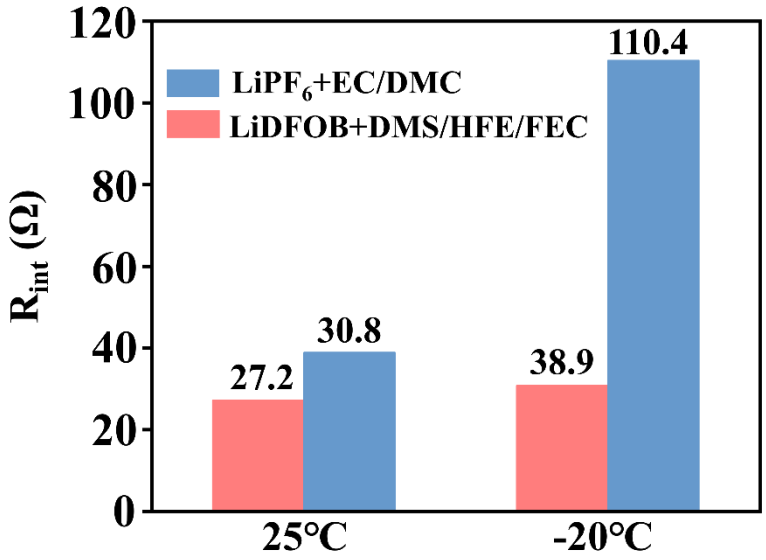

Figure S8. Comparison of EIS impedance of different electrolytes.

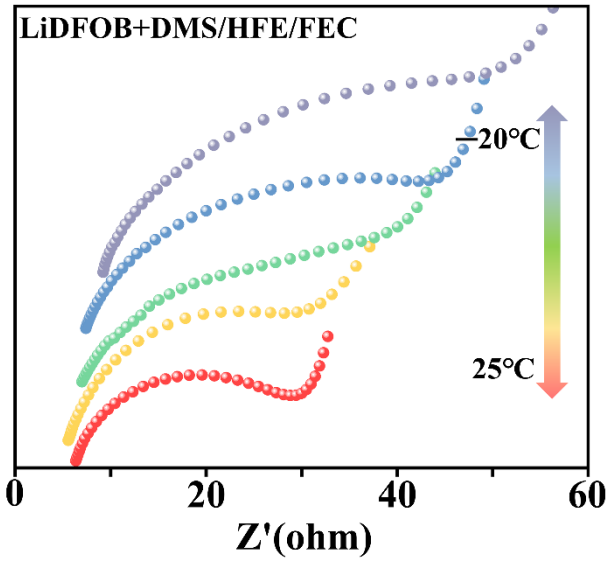

Figure S9. Temperature-dependent EIS spectra of LiDFOB+DMS/HFE/FEC electrolyte.

Table S2. Temperature-dependent fitted impedance parameters of the LiDFOB+DMS/HFE/FEC electrolyte.

Temperature (°C)	R_s (Ω)	R_{int} (Ω)	Ea (kJ mol^{-1})
25°C	3.5	22.8	
10°C	4.9	26.2	
0°C	5.1	30.7	8.9
-10°C	6.2	35.4	
-20°C	7.1	42.7	

Supplementary note: The R_{int} values shown in Figure S8 were obtained from cells measured at 25 and −20°C. Table S2 and S3 summarize independent multi temperature impedance datasets acquired for the Arrhenius analysis, which accounts for the modest numerical differences between the two sets of fitted values.

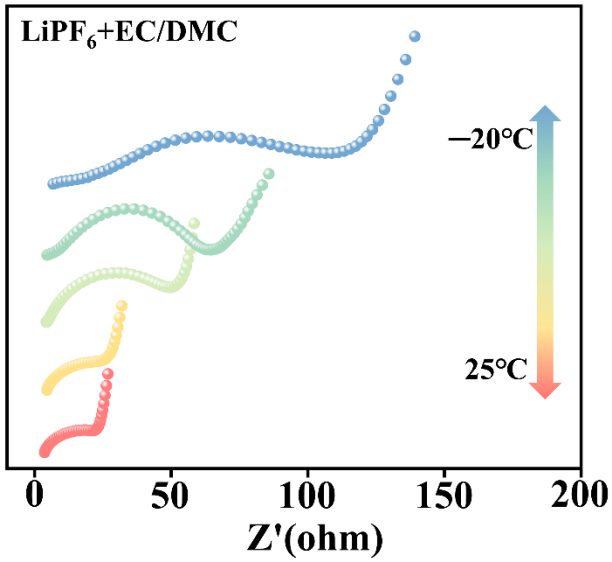

Figure S10. Temperature-dependent EIS spectra of $LiPF_6$+EC/DMC electrolyte.

Table S3. Temperature-dependent fitted impedance parameters of the $LiPF_6$+EC/DMC electrolyte.

Temperature (°C)	R_s (Ω)	R_{int} (Ω)	Ea (kJ mol^{-1})
25°C	4.56	27.4	
10°C	5.37	33.8	
0°C	6.12	47.5	20.6
-10°C	8.79	68.4	
-20°C	12.85	118.7	

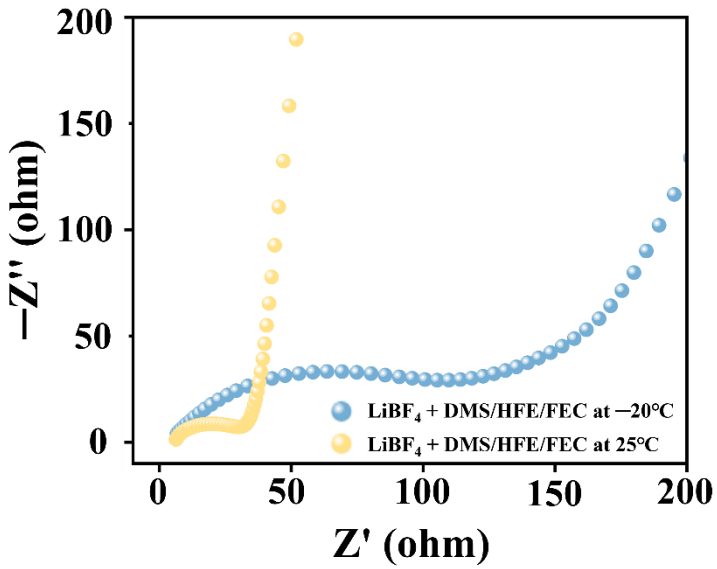

Figure S11. Nyquist plots for $LiBF_4$+DMS/HFE/FEC at 25 and −20°C.

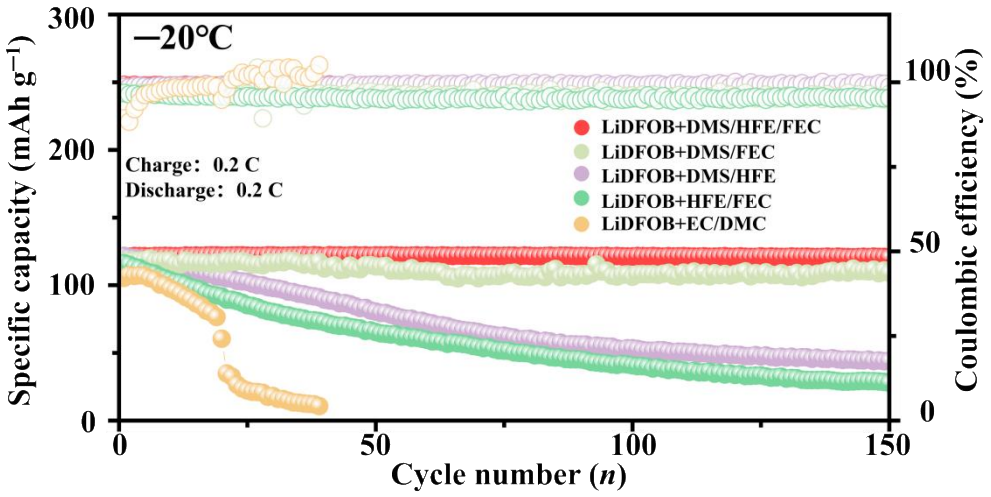

Figure S12. Electrochemical performance of $LiCoO_2$||Li cells using different electrolytes.

Supplementary note: Figure S12 compares the low-temperature cycling performance of $LiCoO_2$||Li cells using different LiDFOB-based electrolytes at −20°C. The conventional LiDFOB+EC/DMC electrolyte shows rapid capacity decay within the initial cycles, together with a pronounced decrease in Coulombic efficiency, indicating sluggish ion transport and unstable interfacial chemistry under subzero conditions. In sharp contrast, the electrolyte containing DMS, HFE, and FEC delivers the most stable cycling behavior. The LiDFOB+DMS/HFE/FEC electrolyte maintains a reversible capacity of 120.6 mAh g^{-1} over 150 cycles at 0.2 C, with Coulombic efficiency remaining close to 100%, demonstrating its superior compatibility with low-temperature $LiCoO_2$||Li operation. The comparison among electrolytes with different solvent/additive combinations further highlights the synergistic role of DMS, HFE, and FEC. The LiDFOB+DMS/FEC electrolyte still provides moderate capacity retention, but its capacity is lower than that of the DMS/HFE/FEC system. In contrast, electrolytes lacking either FEC or DMS suffer from more obvious capacity fading, suggesting that the ternary solvent/additive combination is essential for maintaining fast ion transport and stable electrode/electrolyte interfaces at −20°C. DMS contributes to salt dissolution and low-temperature ionic conduction, HFE helps reduce viscosity and improve fluidity, while FEC promotes the formation of a robust interphase. As a result, the LiDFOB+DMS/HFE/FEC electrolyte achieves the best balance between capacity retention, cycling stability, and Coulombic efficiency under low-temperature conditions.

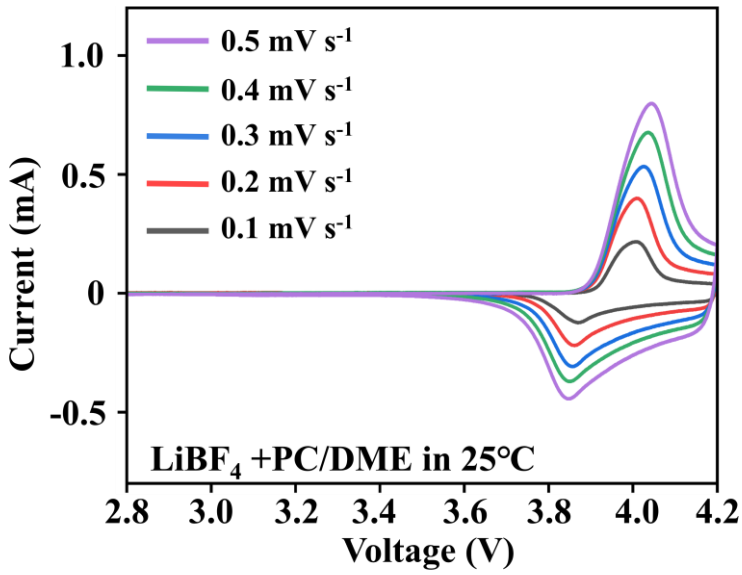

Figure S13. CV curves of $LiCoO_2$||Li cells using the $LiBF_4$+PC/DME electrolyte, recorded at 25°C over 2.8–4.2 V at scan rates of 0.1–0.5 mV s^{-1}.

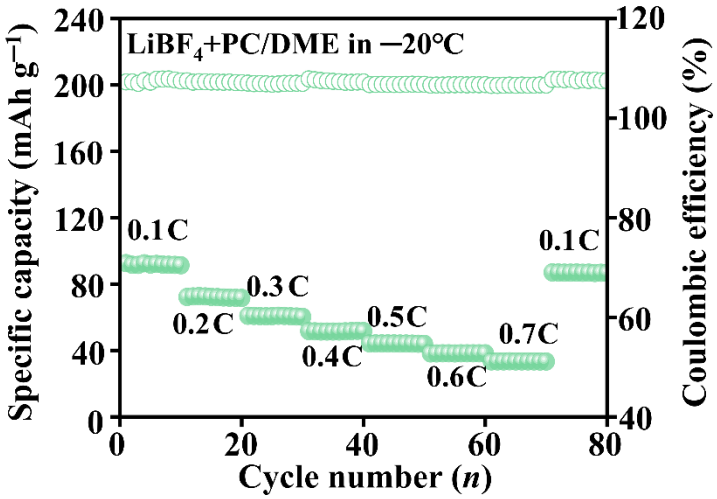

Figure S14. Rate capability and corresponding coulombic efficiency with $LiBF_4$-based electrolyte at –20°C.

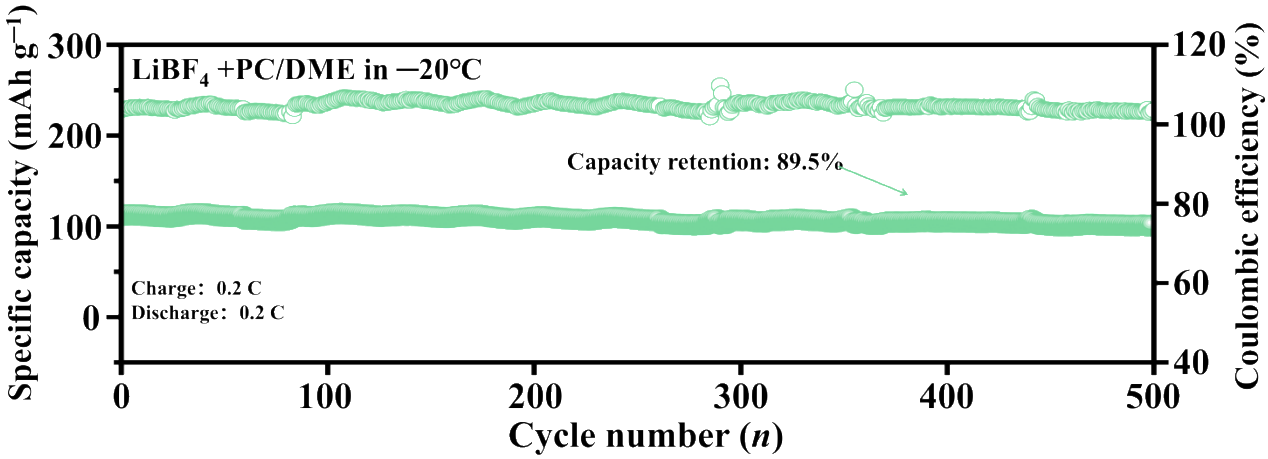

Figure S15. Long-term cycling performance of $LiCoO_2$||Li cell with $LiBF_4$+PC/DME electrolyte at –20°C.

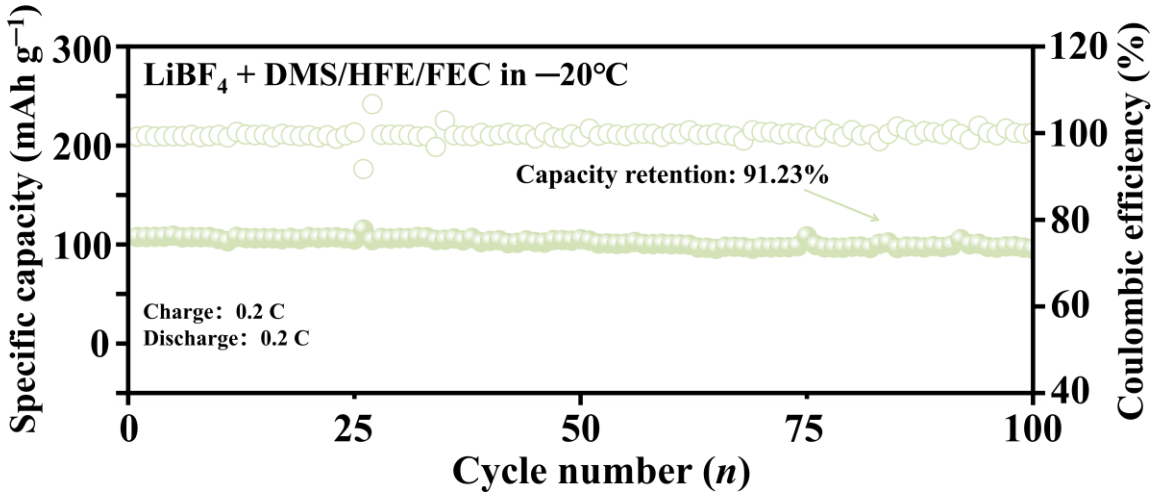

Figure S16. Cycling performance and Coulombic efficiency of $LiCoO_2$||Li cell with $LiBF_4$ + DMS/HFE/FEC electrolyte at –20°C.

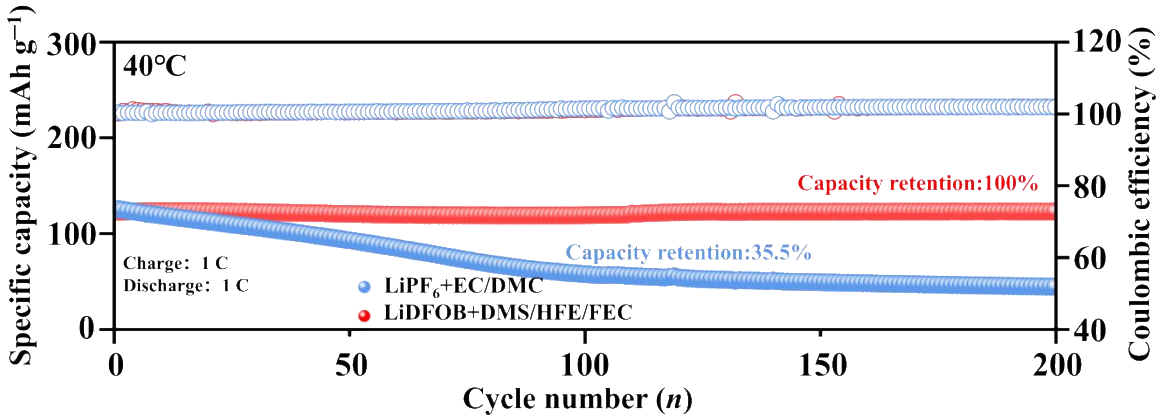

Figure S17. Long-term cycling performance of $LiCoO_2$||Li cell with different electrolytes at 40°C.

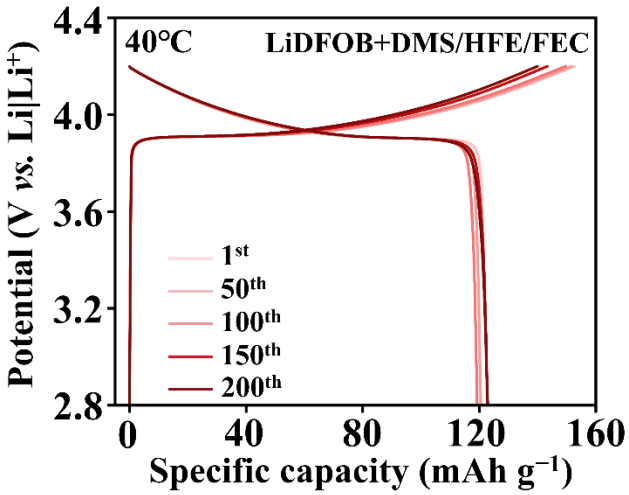

Figure S18. Corresponding charge/discharge curves with LiDFOB+DMS/HFE/FEC electrolyte at 40°C.

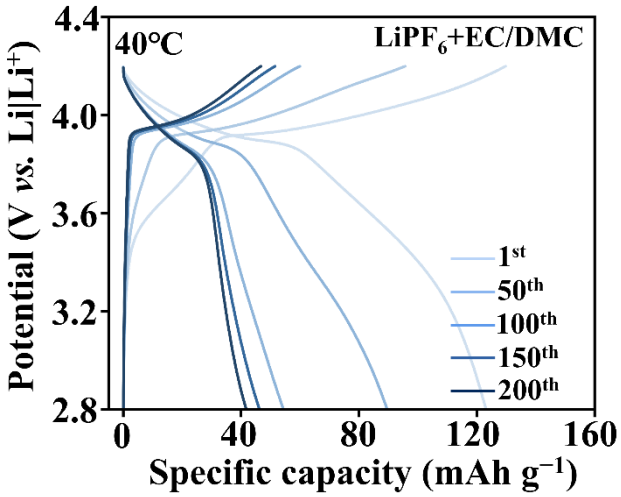

Figure S19. Corresponding charge/discharge curves with $LiPF_6$+EC/DMC electrolyte at 40°C.

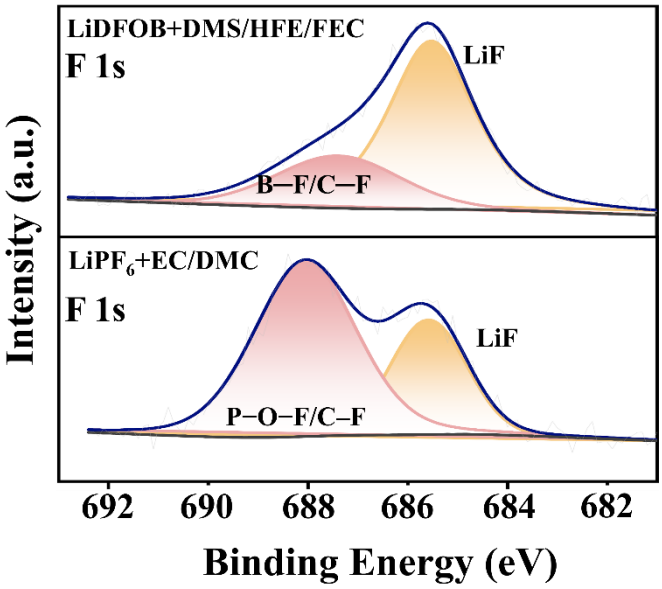

Figure S20. XPS spectra of F 1s for lithium anode after cycling in both electrolytes.

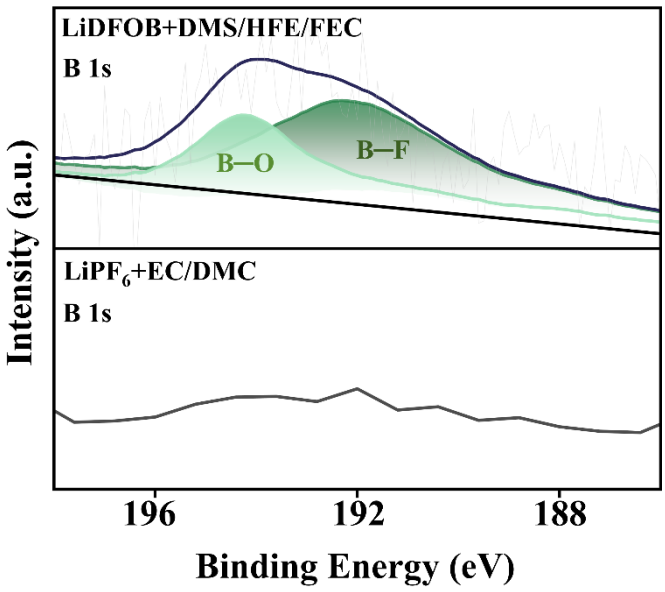

Figure S21. XPS spectra of B 1s for $LiCoO_2$ cathode after cycling in both electrolytes.

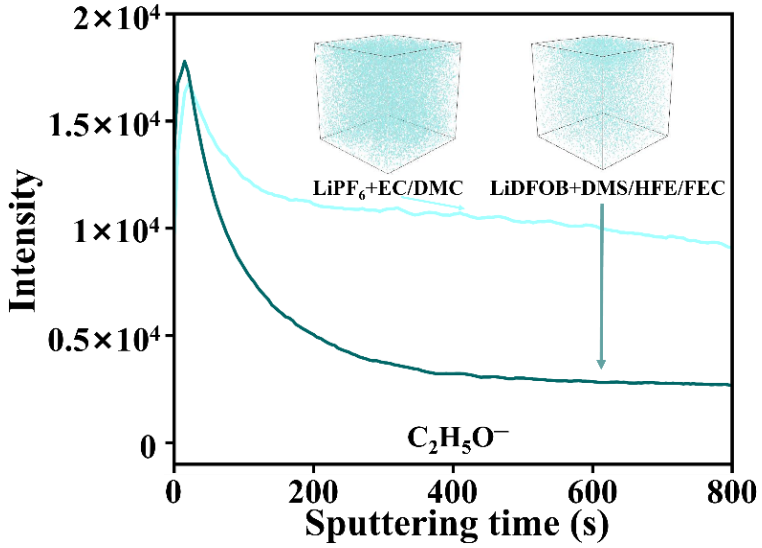

Figure S22. The 3D TOF-SIMS rendering images illustrate the distribution of $C_2H_5O^-$ for cycled graphite anode and corresponding depth sputtering profiles using different electrolytes.

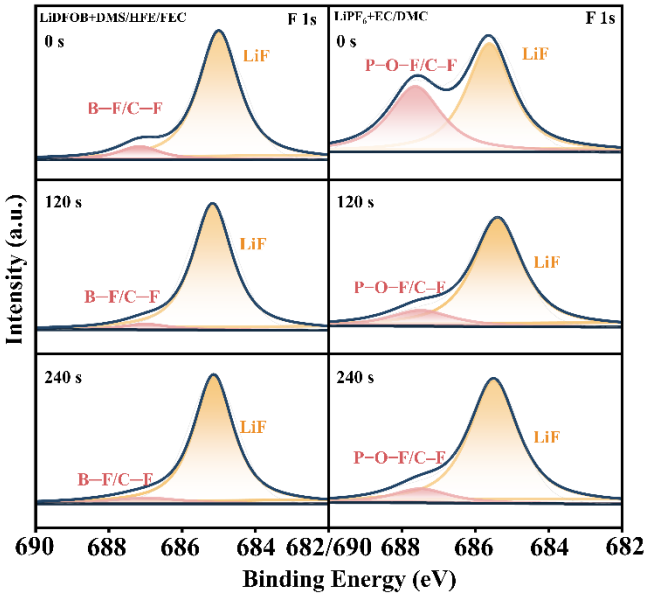

Figure S23. Depth-profiling F 1s XPS spectra of the graphite anode at different sputtering times.

Table S4 Detailed fitting parameters of F 1s XPS spectra for cycled Li metal and graphite electrodes.

Electrolyte	Electrode	Assignment	Binding energy (eV)	FWHM (eV)	Area (%)	Background	Peak shape
LiDFOB + DMS/HFE/ FEC	Li metal	LiF	685.50	1.38	73.36 %	Shirley	Gaussian-Lorentzian
		B–F/C–F	687.52	1.83	26.64 %	Shirley	Gaussian-Lorentzian
	Graphite-0 s	LiF	685.50	1.32	90.52 %	Shirley	Gaussian-Lorentzian
		B–F/C–F	687.58	1.35	9.48 %	Shirley	Gaussian-

	Graphite-120 s	LiF	685.50	1.31	95.01 %	Shirley	Lorentzian Gaussian-Lorentzian
		B–F/C–F	687.48	1.48	4.99 %	Shirley	Gaussian-Lorentzian
	Graphite-240 s	LiF	685.50	1.30	91.81 %	Shirley	Gaussian-Lorentzian
		B–F/C–F	687.54	1.82	8.19 %	Shirley	Gaussian-Lorentzian
	Li metal	LiF	685.55	1.42	30.62 %	Shirley	Gaussian-Lorentzian
		P−F/P−O−F/C–F	687.63	1.98	69.38 %	Shirley	Gaussian-Lorentzian
$LiPF_6$+EC/DMC	Graphite-0 s	LiF	685.52	1.45	59.32 %	Shirley	Gaussian-Lorentzian
		P−F/P−O−F/C–F	687.58	1.68	40.68 %	Shirley	Gaussian-Lorentzian
	Graphite-120 s	LiF	685.48	1.44	84.23 %	Shirley	Gaussian-Lorentzian
		P−F/P−O−F/C–F	687.55	1.87	15.77 %	Shirley	Gaussian-Lorentzian
	Graphite-240	LiF	685.51	1.62	88.31 %	Shirley	Gaussian-

	s					Lorentzian Gaussian-Lorentzian
		P–F/P–O–F/C–F	687.61	1.82	11.69 %	Shirley

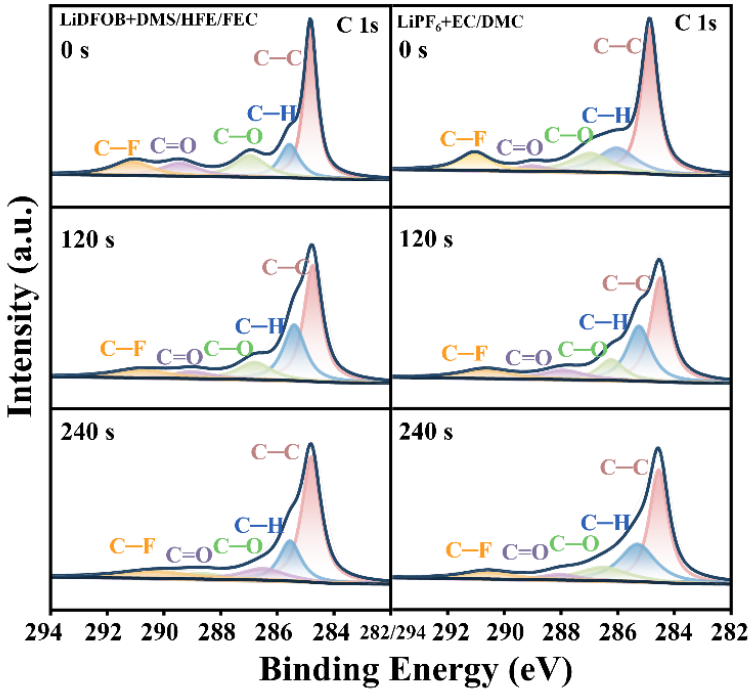

Figure S24. Depth-profiling C 1s XPS spectra of the $LiCoO_2$ cathode at different sputtering times.

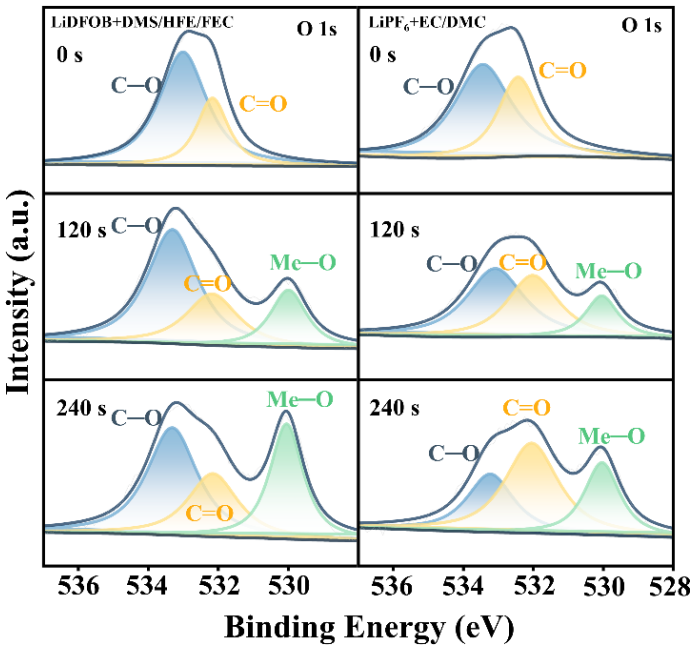

Figure S25. Depth-profiling O 1s XPS spectra of the $LiCoO_2$ cathode at different sputtering times.

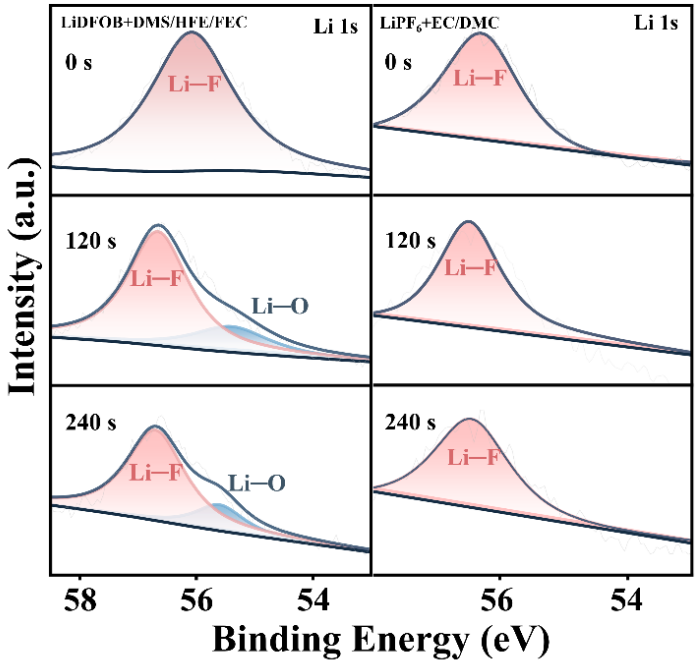

Figure S26. Depth-profiling Li 1s XPS spectra of the $LiCoO_2$ cathode at different sputtering times.

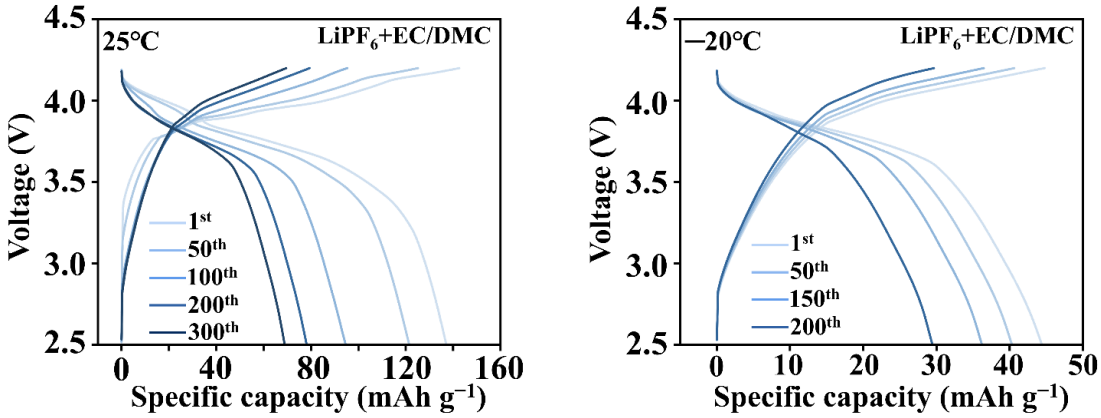

Figure S27. Charge/discharge profiles of $LiCoO_2$||graphite full cells with $LiPF_6$+EC/DMC electrolyte at 25 and −20°C.

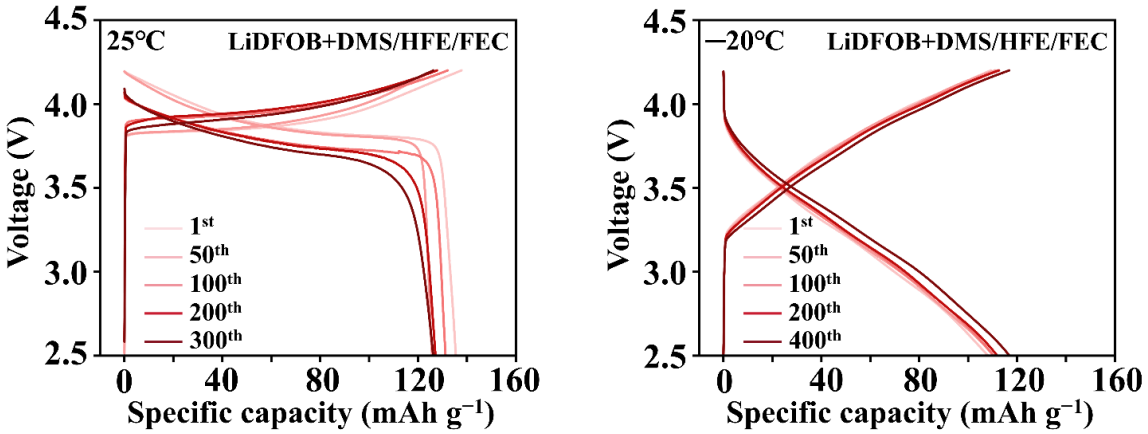

Figure S28. Charge–discharge profiles of $LiCoO_2$||graphite full cells with LiDFOB+DMS/HFE/FEC electrolyte at 25 and −20°C.

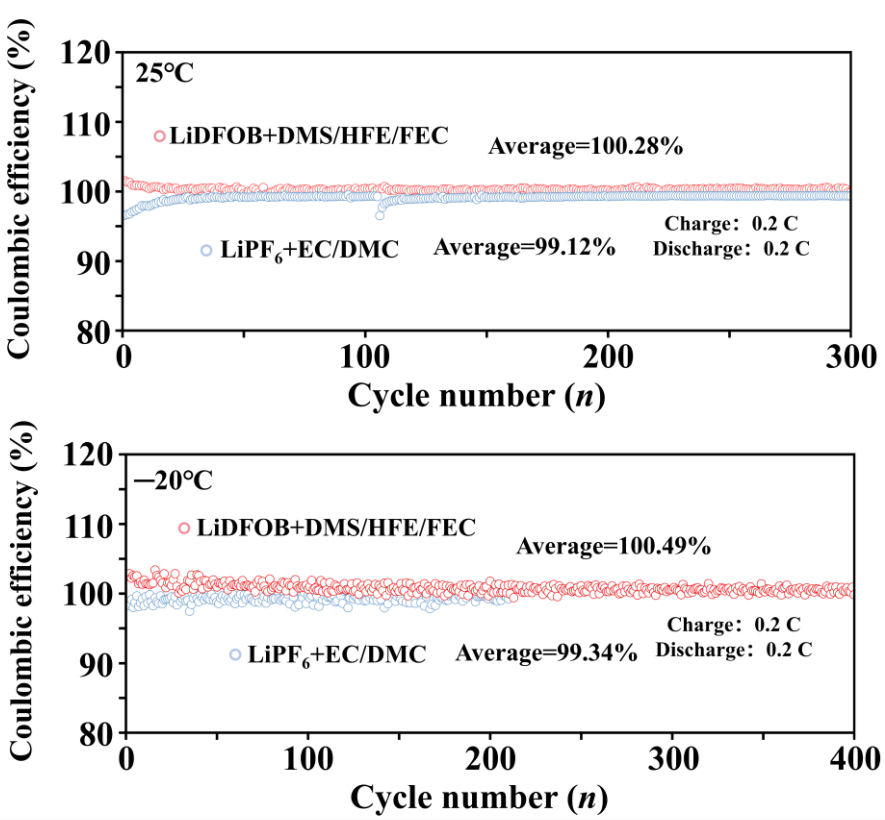

Figure S29. Coulombic efficiency profiles of $LiCoO_2$||graphite full cells with $LiPF_6$+EC/DMC and LiDFOB+DMS/HFE/FEC electrolytes at 25 and −20°C.

Figure S30. Visual observation of LiDFOB+DMS/HFE/FEC electrolyte at −20°C.

Table S5 Low-temperature performance comparison of LIBs.

Electrolyte	System	Performance	Ref.
1.5 M LiDFOB in DMS/HFE/FEC = 5:4:1 v/v/v	$LiCoO_2$||Li	95.1% after 500 cycles, −20°C, 0.2 C	This work
1.5 M LiDFOB in DMS/HFE/FEC = 5:4:1 v/v/v	$LiCoO_2$||graphite	Stable after 400 cycles, −20°C, 0.2 C	This work
$LiBF_4$ + PC/DME	$LiCoO_2$||Li	89.5% after 500 cycles, −20°C, 0.2 C	Comparison in this work
0.4 M LiDFOB + 0.6 M LiFSI in DMS	$LiCoO_2$||graphite	90% after 850 cycles, −20°C, 2 C	[1]
1 M $LiPF_6$ in EC: DMC = 1:1 vol. + 1.0% Li-SiSB + 0.2% PDMS-HT	$LiCoO_2$||graphite	84.6% after 50 cycles, −20°C, 0.1 C	[2]
1.3 M LiFSI-DME/TFEE (2:8 by vol) + 1% LiFMDFB + 0.05% $AgNO_3$	$LiCoO_2$||Li	79.3% after 300 cycles, − 20°C, 0.2 C	[3]
1 M $LiPF_6$ in EC/DMC/IF (3:7:8.2, v/v/v) with FEC additive	$LiCoO_2$||Li	66.7% after 200 cycles, − 20°C, 0.3 C	[4]
1 M $LiPF_6$/MTFP	$LiCoO_2$||Li	96% after 50 cycles, − 20°C, 0.1 C	[5]

REFERENCES

1. Zhao Y, Hu Z, Zhao Z, et al. Strong solvent and dual lithium salts enable fast-charging lithium-ion batteries operating from -78 to 60°C. J. Am. Chem. Soc. 2023;145(40):22184–22193. DOI:10.1021/jacs.3c08313.
2. Phiri I, Ko S, Kim S, et al. Zwitterionic osmolyte-inspired additives as scavengers and low temperature performance enhancers for lithium ion batteries. Mater. Lett. 2021;288:129366. DOI:10.1016/j.matlet.2021.129366.
3. Kim S, Lee J-A, Lee TK, et al. Wide-temperature-range operation of lithium-metal batteries using partially and weakly solvating liquid electrolytes. Energy Environ. Sci. 2023;16(11):5108–5122. DOI:10.1039/D3EE02106H.
4. Liu J, Yuan B, He N, et al. Reconstruction of Lif-rich interphases through an anti-freezing electrolyte for ultralow-temperature $LiCoO_2$ batteries. Energy Environ. Sci. 2023;16(3):1024–1034. DOI:10.1039/D2EE02411J.
5. Ugata Y, Yukishita K, Kazahaya N, Takahashi S, Yabuuchi N. Nonflammable

fluorinated ester-based electrolytes for safe and high-energy batteries with $LiCoO_2$. Chem. Mater. 2023;35(9):3686–3693. DOI:10.1021/acs.chemmater.3c00374.